Phase and microstructural development in alumina sol–gel coatings on CoCr alloy

I. J. BAE, O. C. STANDARD*
School of Materials Science and Engineering, The University of New South Wales, UNSW, Sydney, NSW 2052, Australia
E-mail: o.standard@unsw.edu.au

G. J. ROGER, D. BRAZIL
Australian Surgical Design and Manufacture P/L, Unit 2, 12 Frederick Street, St. Leonards, NSW 2065, Australia

Phase transformation of γ-Al_2O_3 to α-Al_2O_3 in alumina sol gel coatings on biomedical CoCr alloy was studied as function of heat treatment temperature and time. Transformation in unseeded coatings was significant only above $\sim 1200\,^{\circ}C$. Addition of α-Al_2O_3 seed particles having an average size of approximately 40 nm lowered the phase transformation temperature to around 800 °C. These particles were considered to act as heterogeneous nucleation sites for epitaxial growth of the α-Al_2O_3 phase. The kinetics and activation energy (420 kJ/mol) for the phase transformation in the seeded coatings were similar to those reported for seeded monolithic alumina gels indicating that the transformation mechanism is the same in the two material configurations. Avrami growth parameters indicated that the mechanism was diffusion controlled and invariant over the temperature range studied but that growth was possibly constrained by the finite size of the seed particles and/or coating thickness. The phase transformation occurred by the growth of α-Al_2O_3 grains at the expense of the precursor fine-grained γ-Al_2O_3 matrix and near-complete transformation coincided with physical impingement of the growing grains. The grain size at impingement was ~ 100 nm which agreed well with that predicted from the theoretical linear spacing of seed particles in the initial sol.

1. Introduction

CoCr alloys are used extensively for load-bearing and articulating orthopedic applications, such as knee and hip prostheses, owing to their acceptable biocompatibility, excellent strength and toughness, and reasonable hardness. In these applications, CoCr usually articulates against a polymer counter-surface of ultrahigh molecular weight polyethylene (UHMWPE). This wear couple produces micron-sized UHMWPE wear debris which is considered to be a primary cause of osteolysis and eventual aseptic loosening of these prostheses [1–5].

The wear rate of UHMWPE against alumina (α-Al_2O_3) is significantly lower than that against CoCr alloys [6–10]. As a result, the incidence of aseptic loosening tends to be lower with alumina–UHMWPE wear couples [11]. It follows that the wear performance of orthopedic implants may be improved, and the incidence of aseptic loosening reduced, by incorporating α-Al_2O_3 as the counter-surface against UHMWPE [7]. However, with the notable exception of alumina femoral heads, monolithic ceramics cannot be used as load-bearing orthopedic prostheses owing to their low fracture toughness and brittle mode of failure. Instead, biomedical load-bearing applications of ceramics are restricted mainly to coatings on metal prostheses.

CoCr alloys, in particular, have a highly coherent passivation layer of Cr_2O_3 [12, 13] that imparts excellent corrosion resistance to the alloy. Cr_2O_3 and α-Al_2O_3 have similar hexagonal (corundum) crystal structures and, according to phase diagrams of the Cr_2O_3-Al_2O_3 system [14–16], have complete solid solubility in each other at high temperatures ($> 950\,^{\circ}C$). At lower temperatures, there exists a miscibility gap in which two solid solution corundum phases (i.e. an alumina-rich phase and a chromia-rich phase) coexist. The high degree of mutual solubility is significant because it suggests that it may be possible to form a compositionally graded interdiffusion interface between an α-Al_2O_3 coating and CoCr substrate during heat-treatment. Such an interface is important for two reasons. First, the thermal expansion coefficient varies monotonically from α-Al_2O_3 $(8.4 \times 10^{-6}\,^{\circ}C^{-1})$ to Cr_2O_3 $(9.6 \times 10^{-6}\,^{\circ}C^{-1})$ to CoCr $(14.0 \times 10^{-6}\,^{\circ}C^{-1})$ such that on cooling after heat-treatment (i.e., for coating processes involving heat-treatment) there is a gradual rather than an abrupt change in the extent of contraction of the coating ''layers''. Also,

*Author to whom all correspondence should be addressed.

the magnitudes of the thermal expansion coefficients indicate that the ceramic coating should be placed in a state of compression. Second, the elastic modulus varies monotonically from α-Al_2O_3 (380 GPa) to Cr_2O_3 (325 GPa) to CoCr (240 GPa) which may help to minimize the stress discontinuity across the interface. Stress discontinuities are undesirable because they can cause interfacial cracking and delamination of the coating from the substrate during mechanical loading. Thus, the interdiffusion bond layer, combined with graduation of residual stresses and minimization of stress discontinuities, may promote strong adherence of α-Al_2O_3 coatings to CoCr.

Sol–gel processing is a common method used for the deposition of alumina coatings. The initial sol–gel precursor phase, usually boehmite (γ-AlOOH) or gibbsite (γ-$Al(OH)_3$), comprising the deposited coating is converted by heat-treatment to α-Al_2O_3 via several possible phase transformation sequences involving alumina transition phases [17]. The final stable phase of α-Al_2O_3 is obtained at temperatures above $\sim$ 1200 °C [18–20]. Nanometer-sized α-Al_2O_3 seed particles can be incorporated into the unfired sol–gel precursor to promote heterogeneous nucleation of the α-Al_2O_3 phase thereby lowering significantly the temperature needed for the transformation of the alumina precursor phase to α-Al_2O_3 [21–24], as well as for densification of the coating [25, 26]. This addresses a major constraint in the processing of coatings on CoCr in that any heat-treatment should be done below $\sim$ 1200 °C in order to avoid degradation of the microstructure and mechanical properties of CoCr [27].

Sol–gel deposition of alumina coatings on CoCr has been investigated by the authors in terms of sol–gel processing parameters; phase evolution, densification, and grain growth of the coating; coating–substrate interdiffusion; and resultant mechanical properties and wear behavior [28]. In this paper, a study of the effect of heat-treatment conditions (temperature and time) and addition of nanometer-sized α-Al_2O_3 seed particles on α-Al_2O_3 phase evolution in boehmite-derived sol-gel coatings is presented.

2. Experimental procedure

2.1. Preparation of Al_2O_3-coated CoCr alloy

Surgical grade CoCr alloy [29] (ASDM, St Leonards, Australia) having a nominal composition of 60 wt % Co, $\sim$ 27–30 wt % Cr, $\sim$ 5–7 wt % Mo, and small amounts of Fe, Ni, Si, Mn, and C comprising the balance, was used as the substrate. Disks (10 mm diameter, 2 mm thickness) were polished on one face to a surface roughness (R_a) of $\sim$ 0.01 μm using diamond-impregnated rotating polishing cloths. After polishing, the disks were degreased in acetone, cleaned ultrasonically in deionized water, and stored in absolute ethanol until coating.

A boehmite (γ-AlOOH) sol was prepared by the method reported by Yoldas [30]. Briefly, 1 mol of aluminum tri-*sec*-butoxide ($Al(C_4H_9)_3$; 99.0 wt % purity, Aldrich Chemical Company, Milwaukee, USA) was hydrolyzed by mixing with 100 mol of deionized water, followed by vigorous stirring at 90 °C. This solution was peptized by adding 0.2 mol of nitric acid (HNO_3) followed by stirring at 90 °C for 48 h. The resultant boehmite sol was completely transparent and had a final pH of $\sim$ 3.0.

Nanometer-sized seed particles of α-Al_2O_3, for promoting heterogeneous nucleation and growth of α-Al_2O_3 in the coating during heat-treatment, were prepared from a commercial alumina powder (99.99% purity; 0.2 μm crystallite size; Taimei Chemical Co. Ltd., Nagano, Japan). The powder was deagglomerated by ball-milling in deionized water for 48 h using high-purity α-Al_2O_3 grinding balls (99.7% purity, Aston Co. Ltd., Incheon, South Korea) in a high-density polyethylene mill chamber. The resultant suspension was allowed to settle for 30 days, after which time the supernatant containing α-Al_2O_3 nanoparticles was collected. Examination of the nanoparticles using transmission electron microscopy (TEM; Philips CM200, FEI Co., Hillsboro, Oregon, USA) showed them to be relatively equiaxed with diameters in the range of $\sim$ 10–100 nm with an average size of $\sim$ 40 nm. These dimensions are similar to those of seed particles used in other studies of heterogeneous nucleation and crystallization of alumina sols [21–26]. The zeta potential of the nanoparticles in deionized water was measured as a function of pH using electrophoretic light scattering (ZetaPlus, Brookhaven Instruments Corp., Holtsville, USA). The zeta potential was maximal ($\sim$ 55 mV) at pH 3–4 indicating that the nanoparticles should have maximal repulsion, and thus low tendency to agglomerate or settle, when incorporated into the boehmite sol.

The CoCr disks were coated with either pure boehmite sol or boehmite sol seeded with α-Al_2O_3 nanoparticles. The concentration of nanoparticles in the latter was 2.5 wt % (dry basis) of the sol, which was shown from preliminary work [28] to be optimal in terms of eliminating cracking during drying whilst providing heterogeneous nucleation of α-Al_2O_3 phase during heat-treatment. This concentration was similar to that used in transformation studies of seeded monolithic boehmite sols [21, 25, 27]. The viscosity of the sol suspensions was increased to $\sim$ 200 mPa s by increasing the solids loading through evaporation of water at 80 °C. This viscosity was known, from pilot studies, to be an optimum between having a sufficiently low viscosity for satisfactory spin coating, and having a sufficiently high solids loading for reducing drying shrinkage and avoiding cracking of the deposited coating. Sols were deposited onto the CoCr alloy disks by spin coating at $\sim$ 1500 rpm for 3 min. The coated disks were dried in air, initially at 25 °C and then at 100 °C. The dried coatings were calcined at 450 °C in air for 0.5 h.

Coated samples were heat-treated in air using a horizontal tube furnace equipped with an alumina working tube (Ceramic Engineering Furnace Manufacturers, Marrickville, Australia). Heat-treatment temperatures and times varied according to the experiments specified below. A heating rate of 600 °C/h was used in all experiments. A micrograph (obtained by field emission scanning electron microscopy; S4500, Hitachi, Tokyo, Japan) of a polished cross-section of a heat-treated sample is shown in Fig. 1. The fired coatings were $\sim$ 3–4 μm thick and of high bulk density, appeared

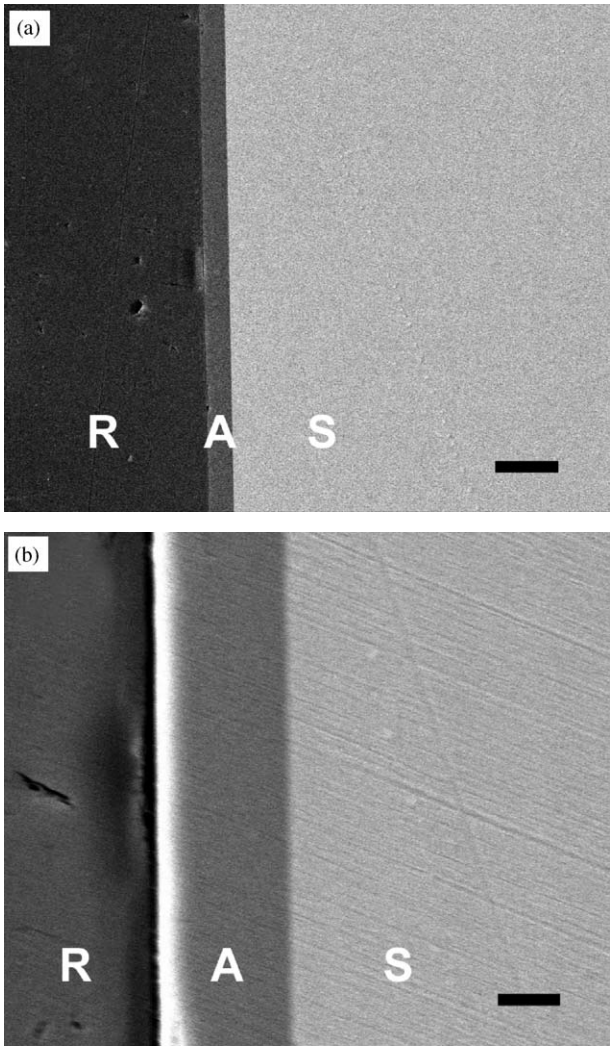

Figure 1 Micrographs of the polished cross-section of a seeded coating heat-treated at 800 °C for 8 h at (a) low magnification (scale bar = 10 μm) and (b) high magnification (scale bar = 2 μm). R, A, and S denote resin mount, alumina coating, and CoCr substrate, respectively.

to be well attached to the CoCr substrate, and were free from drying or firing cracks.

2.2. Characterization of phase composition of coatings

The evolution of α-Al_2O_3 in unseeded and seeded coatings was studied as function of heat-treatment temperature (up to 1200 °C) and time (up to 128 h). The phase composition of coatings heat-treated *in situ* on disks was analyzed by thin film X-ray diffraction (XRD; X'Pert PRO MRD, PANalytical, Almelo, The Netherlands) using Cu-Kα radiation and an incident angle of 0.8°. The resultant patterns were relatively low in intensity and provided only qualitative identification of phases.

Quantitative determination of phase composition was done using heat-treated coatings that had been removed from the disks after drying. This provided sufficient quantity of each coating to yield XRD patterns of reasonable intensity for quantification. Coatings was analyzed using a powder-type X-ray diffractometer (PW1140, Philips Co., Ltd, Eindhoven, The Netherlands) employing Cu-Kα radiation. The fraction of transformed α-Al_2O_3 phase in each coating was calculated as the integrated intensity of the major α-Al_2O_3 diffraction peak ($\{1\,1\,3\}$ reflection) of the coating expressed as a fraction of the integrated intensity of the corresponding peak of a reference sample consisting entirely of α-Al_2O_3. This reference sample was prepared by heat-treating an unseeded coating at 1600 °C (this temperature being well in excess of that needed to give a complete transformation of boehmite coatings [23, 25]) and its XRD pattern was virtually identical to that measured for the commercial α-Al_2O_3 powder used to prepare the seed particles.

The rate constant (k) of the γ-Al_2O_3 (this phase is present after calcining at 450 °C) to α-Al_2O_3 phase transformation at each temperature was determined by fitting the α-Al_2O_3 fraction (f) versus time (t) data to the Avrami growth equation [31]:

$$f = 1 - \exp(-kt^n) \quad (1)$$

where n is a temperature-independent exponent. The activation energy (E_a) of the phase transformation was determined by fitting the rate constant (k) versus temperature (T) data to the Arrhenius relationship [31]:

$$k = k_0 \exp(E_a/(RT)) \quad (2)$$

where k_0 is a constant and R is the gas constant.

The grain morphology in selected coatings was examined qualitatively by TEM (CM200, Philips, Eindhoven, The Netherlands). To avoid the technically demanding and time-consuming task of preparing thin sections of ceramic coatings on metals, coatings were removed from their substrates after drying. The coatings were then calcined and heat-treated (750–900 °C up to 96 h) as described for the coated samples. The resultant flakes were fractured to yield thin edges for TEM examination.

3. Results

A selected thin film XRD pattern (seeded coating heat-treated at 800 °C for 8 h) is shown in Fig. 2. CoCr was identified as the major phase in all samples. The alumina phase evident in the patterns was α-Al_2O_3 and the diffraction intensity of this phase was always much lower than that of CoCr. The intensity of the α-Al_2O_3 peaks

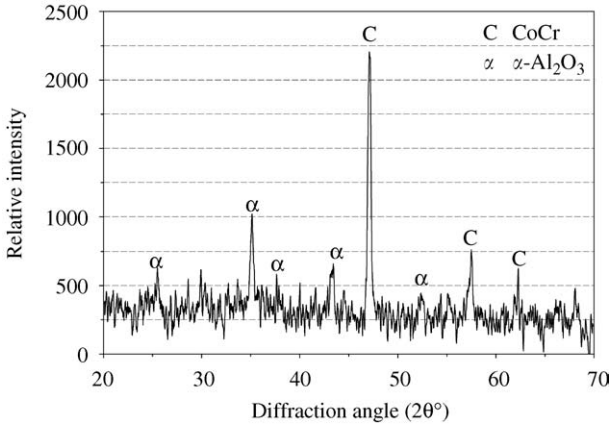

Figure 2 Thin film XRD pattern of a seeded coating heat-treated at 800 °C for 8 h.

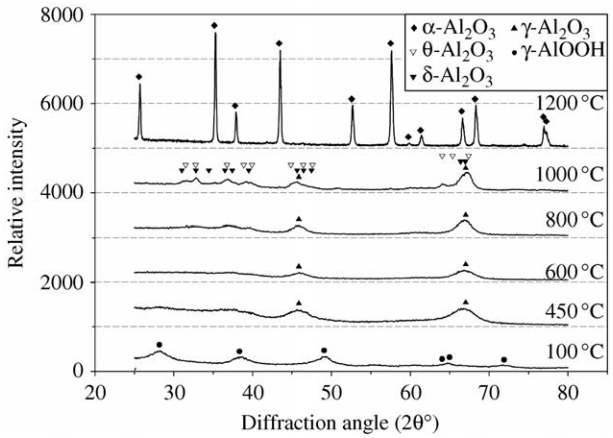

Figure 3 Powder XRD patterns of unseeded coatings after drying at 100 °C, calcining at 450 °C for 30 min, and heat-treating at 600–1200 °C for 2 h.

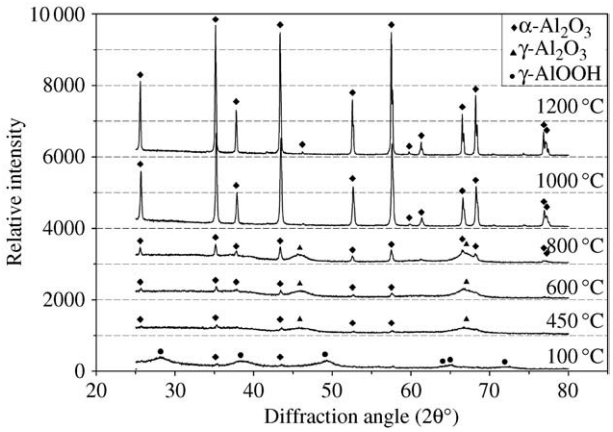

Figure 4 Powder XRD patterns of seeded coatings after drying at 100 °C, calcining at 450 °C for 30 min, and heat-treating at 600–1200 °C for 2 h.

tended to increase with increasing heat-treatment temperature and time whilst the intensity of the CoCr peaks remained constant. Precursor alumina phases that were identified in the powder XRD patterns (see below) were not apparent. However, this is probably a result of the diffraction peaks of phases being of inherently low intensity, because of which the peak was not discernable from the relatively noisy background. Owing to their relatively low intensity, the thin film XRD patterns were unsuitable for quantitative analysis of the alumina phases.

Powder XRD patterns of unseeded coatings (removed from disks prior to heat-treatment) are shown as a function of temperature in Fig. 3. Although difficult to identify with any certainty, the peaks in the dried coating (100 °C) correspond most likely to γ-AlOOH [32] and the peaks in the calcined coating (450 °C) correspond to γ-Al_2O_3 [33]. Above ∼ 900–1000 °C, δ-Al_2O_3 [34] and/or θ-Al_2O_3 [35] were also present in the unseeded coatings. These two polymorphs have similar interplanar spacings and consequently their major peaks occur at similar diffraction angles and, because the measured peaks were broad and of low-intensity, it was not possible to distinguish equivocally between the two phases. The thermodynamically stable phase of α-Al_2O_3 [36] formed in the unseeded coatings at temperatures above ∼ 1100–1200 °C (Fig. 3), in agreement with that reported in the literature [21, 37, 38]. Since such temperatures are considered excessive for the heat-treatment of CoCr [27], futher investigation of the transformation kinetics of unseeded coatings was not done.

Powder XRD patterns of seeded coatings (removed from disks prior to heat-treatment) are shown as a function of temperature in Fig. 4. Peaks corresponding to α-Al_2O_3 [36] are discernable in the dried (100 °C) coating and, given that they are absent in the unseeded coatings, these peaks arise most likely due to the 2.5 wt % α-Al_2O_3 seed particles. As in the unseeded coatings, the precursor γ-AlOOH sol was transformed to γ-Al_2O_3 during calcination at 450 °C. However, unlike the unseeded coatings, γ-Al_2O_3 transformed directly to α-Al_2O_3 during subsequent heat-treatment; the transition alumina phases of δ-Al_2O_3 and/or θ-Al_2O_3 were not apparent in the XRD patterns. Growth of the α-Al_2O_3 phase was evident at temperatures as low as ∼ 700 °C. With increasing heat-treatment temperature and/or time, the intensity of the α-Al_2O_3 diffraction peaks increases and the intensity of the γ-Al_2O_3 peaks decreases, indicating the progressive transformation of γ-Al_2O_3 to α-Al_2O_3. The relative intensities of the α-Al_2O_3 diffraction peaks are similar to indexed values [36] indicating that the α-Al_2O_3 grains were randomly oriented and, specifically, that no significant preferred orientation had occurred on nucleation and growth of the phase within the γ-Al_2O_3 matrix.

The fraction of α-Al_2O_3 in the seeded coatings is plotted as a function of heat-treatment time and temperature in Fig. 5. At a given heat-treatment temperature, the amount of α-Al_2O_3 increased with heat-treatment time. The time to form a given amount of α-Al_2O_3 decreased significantly with increasing temperature. For the time-points used, an incubation period (during which there is no measurable transformation) was not apparent.

The kinetics of the γ-Al_2O_3 to α-Al_2O_3 phase transformation in the seeded coatings (800–950 °C) were fitted to the Avrami growth equation (Equation 1) by plotting $\ln\ln(1/(1-f))$ versus $\ln(t)$. The resultant plots are shown in Fig. 6. At each temperature, the plot was reasonably linear (r^2 values are given in Table I) indicating that the phase transformation in the seeded coatings followed Avrami-type growth kinetics. The values of n and k at each temperature (equal to the slope

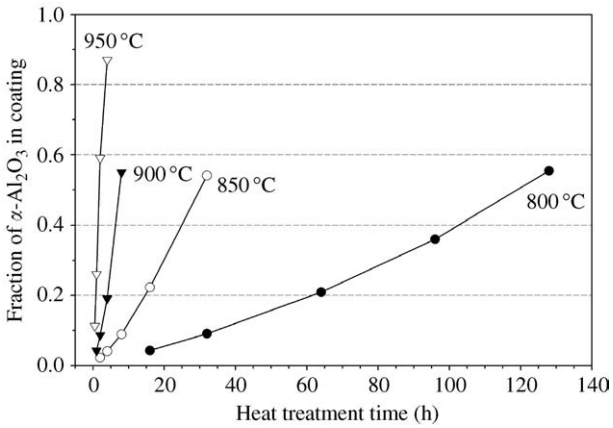

Figure 5 Fraction of transformed α-Al_2O_3 phase in seeded coatings as a function of heat-treatment time at various temperatures.

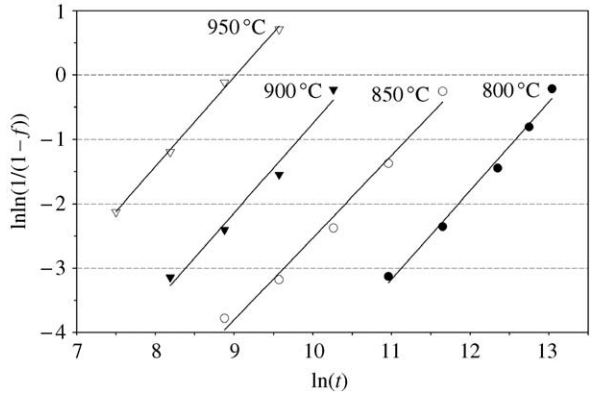

Figure 6 Avrami plot of $\ln\ln(1/(1-f))$ versus $\ln(t)$ for the seeded coatings at various temperatures.

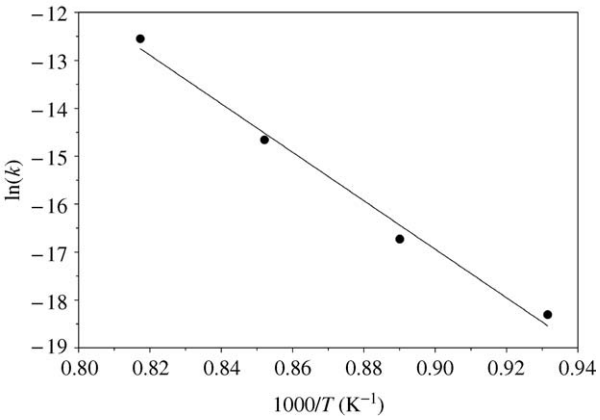

Figure 7 Arrhenius plot of $\ln(k)$ versus $1/T$ for the seeded coatings.

TABLE I Avrami constants, n and k, calculated by regression analysis of the plots in Fig. 7

Temperature (°C)	n	$k(s^{-1})$	r^2
800	1.38	1.12×10^{-8}	0.9895
850	1.28	5.42×10^{-8}	0.9864
900	1.38	4.29×10^{-7}	0.9805
950	1.38	3.54×10^{-6}	0.9976

and exp(intercept) of the plot, respectively) were calculated by linear regression and are given in Table I. The values of n were very similar which suggests that the mechanism of the phase transformation was the same for the four temperatures. The average value of n is 1.36 ($\pm$ 0.05 standard deviation). The rate constant (k) increased with increasing temperature. The Arrhenius plot of $\ln(k)$ versus $1/T$ is shown in Fig. 7. The plot is reasonably linear ($r^2 = 0.9893$) and the activation energy of the γ-Al_2O_3 to α-Al_2O_3 phase transformation was calculated by linear regression to be 420 kJ/mol.

TEM micrographs of coatings heat-treated at 700, 750, 800, 850, and 900 °C for 64 h are shown in Fig. 8. At 700 °C, the coating consisted mostly of a uniform dispersion of fine crystallites which were < 5 nm in size (Fig. 8(a)). From consideration of the XRD pattern for this heat-treatment temperature and time, this phase corresponded to γ-Al_2O_3. At higher temperatures, large grains were also present in the coatings (Fig. 8(b)–(e)). Qualitatively, the concentration of the large grains increased, and the concentration of the fine-grained γ-Al_2O_3 matrix decreased, as the heat-treatment temperature and time increased. Since these microstructural observations correlate well with the evolution of the α-Al_2O_3 phase as determined by XRD, the large grains are most probably α-Al_2O_3. At high α-Al_2O_3 concentrations, the size of the α-Al_2O_3 grains was relatively uniform at each temperature and was invariant over the temperature range studied; this size was estimated from TEM micrographs to be $\sim$ 100 nm.

4. Discussion

The XRD data for the unseeded coatings show that the precursor γ-AlOOH sol was transformed to γ-Al_2O_3 during calcination at 450 °C, then to δ-Al_2O_3 and/or θ-Al_2O_3 at $\sim$ 900–1000 °C, and finally to α-Al_2O_3 above $\sim$ 1100–1200 °C. This transformation sequence is typical of that reported for monolithic unseeded boehmite sols [17, 39]. However, heat-treatment of CoCr should be done below $\sim$ 1200 °C to avoid degradation of the microstructure (most notably, solution annealing resulting in carbide dissolution) and mechanical properties of the alloy [27]. Accordingly, the discussion hereafter focuses on the seeded coatings as they required significantly lower heat-treatment temperatures to obtain the α-Al_2O_3 phase.

In contrast to the unseeded sols, the calcined seeded sols transformed directly from γ-Al_2O_3 to α-Al_2O_3 with the transformation occurring at temperatures as low as $\sim$ 700 °C. This suggests that the α-Al_2O_3 seed particles provided sites for heterogeneous nucleation of the phase transformation. This role of α-Al_2O_3 in alumina transition phases in bulk samples is well demonstrated in the literature [21–26]. Furthermore, it is likely that the initial concentration of nucleation sites was fixed by the concentration of seed particles with each particle providing multiple epitaxial nucleation sites [40–42]. Thus, assuming that no new nucleation sites form (i.e., by homogeneous nucleation in the sol), the phase transformation should proceed solely by epitaxial growth of the α-Al_2O_3 phase on the seed particles. Such heterogeneous growth behavior has been reported for a transition alumina (θ-Al_2O_3) seeded with α-Al_2O_3 nanoparticles [26].

The Avrami growth exponent, n, is determined by the type of nucleation and the geometry of crystal growth and is typically between 1 and 4 [31]. The value of n was largely invariant in the 800–950 °C range (average value of 1.36) indicating that the mechanism of the γ-Al_2O_3 to α-Al_2O_3 phase transformation in the seeded coatings was the same at each temperature. Assuming that the rate of transformation is diffusion-controlled, in this case involving short-range diffusion of Al^{3+} and O^{2-} across the γ-Al_2O_3/α-Al_2O_3 transformation interface [25] (and probably rate-limited by the diffusion of oxygen [26]), the Avrami exponent is given by [43]:

$$n = \beta + 0.5\lambda$$

where β is determined by the type of nucleation and λ is the number of unconstrained orthogonal directions in which the nuclei grow. The absence of any significant incubation period for the γ-Al_2O_3 to α-Al_2O_3 phase transformation suggests that the nucleation sites on the

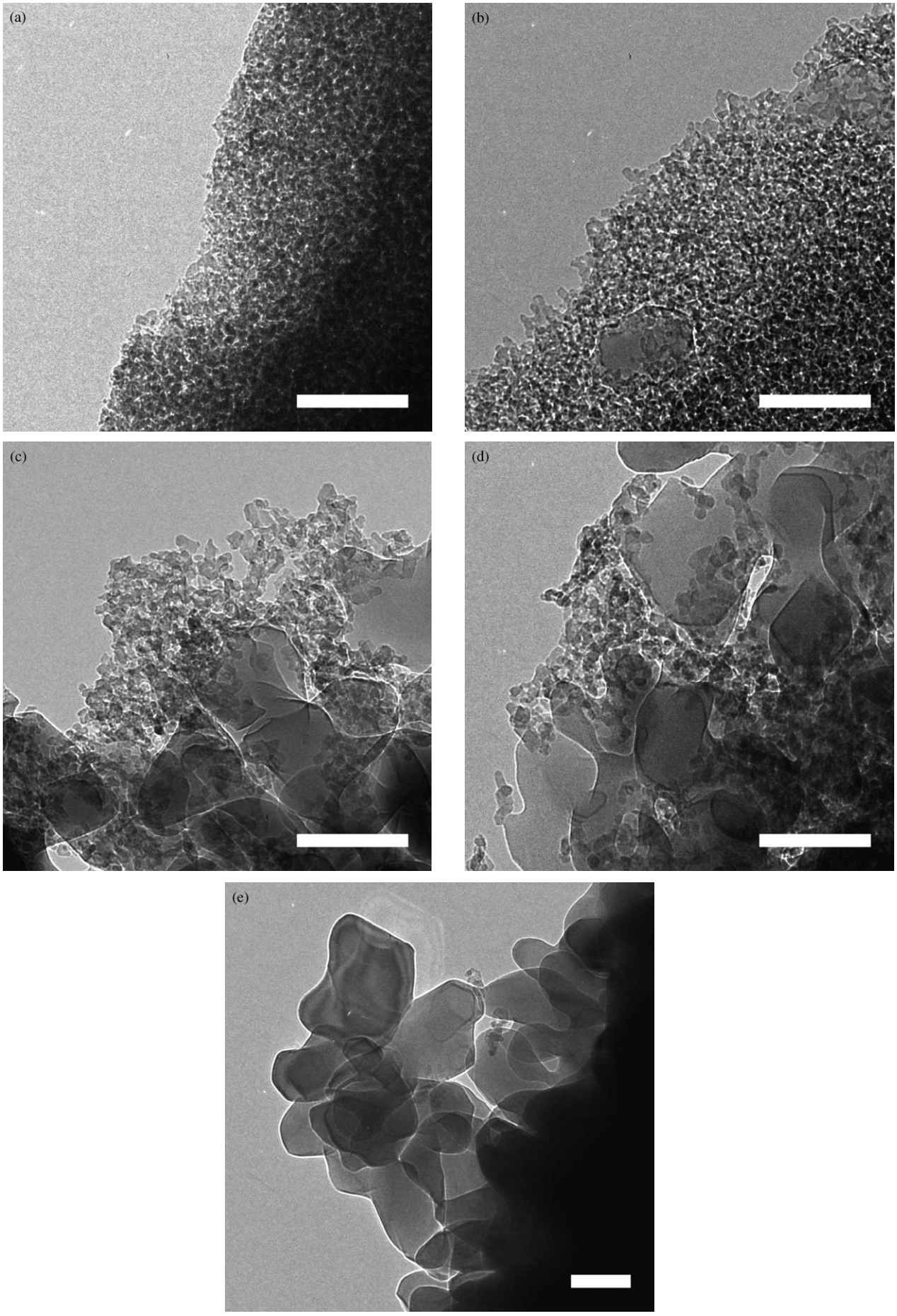

Figure 8 TEM micrographs of seeded coatings heat-treated for 64 h at (a) 700 °C, (b) 750 °C, (c) 800 °C, (d) 850 °C, and (e) 900 °C. Scale bar equals 100 nm.

seed particles became saturated relatively early in the transformation process, in which case β may be taken to be zero [31]. Assuming growth in three directions ($\lambda = 3$), the predicted Avrami exponent for the seeded coatings is therefore 1.5. The measured value of 1.36 agrees reasonably well with this predicted value and with values calculated from kinetic data reported in the literature for transformation at $\sim$ 900–1050 °C of monolithic boehmite gels seeded with particles of α-Al_2O_3 [37, 42] or particles of other oxides having corundum crystal structures [25].

The Avrami exponent for diffusion-controlled transformations may be reduced by boundary conditions such as finite size of the nuclei particles or a finite dimension in one or more given directions [31, 44]. Both of these occur in the present work. Firstly, the average seed size in this work was $\sim$ 40 nm which is significant compared with the final grain size at impingement of $\sim$ 100 nm. The value of *n* for diffusion-controlled growth of nuclei particles having an initial dimension greater than about one tenth of the distance of separation (or one tenth of the dimension of the final particles) is predicted to be between 1 and 1.5 [44]. This may account for the measured *n* value of 1.36 being lower than the predicted value of 1.5. Secondly, in this work, the coatings were $\sim$ 3 μm thick and the transformed α-Al_2O_3 grains were $\sim$ 100 nm in size. Growth across the thickness of the coating was therefore limited to a distance of $\sim$ 30 grains but unrestricted in the other two orthogonal directions. In the limiting case of growth constrained to two directions ($\lambda = 2$), the Avrami exponent for site-saturated nucleation ($\beta = 0$) is predicted to be 1. Thus, it is possible that the measured *n* value was slightly lower than the predicted value due to the growth of the α-Al_2O_3 phase being constrained by the limited thickness of the coatings.

The activation energy of 420 kJ/mol for the γ-Al_2O_3 to α-Al_2O_3 phase transformation in the seeded coatings agrees with published values [40, 42]. This indicates that the transformation in the coatings is not significantly different, either mechanistically or thermodynamically, from that which occurs in monolithic samples. However, the kinetics of the phase transformation were determined for coatings removed from the CoCr substrata before heat-treatment. It is possible that the kinetics of the transformation in coatings heat-treated *in situ* on the CoCr disks could be affected by interaction with the CoCr and the formation of the diffusion bond interface. In particular, it has been shown that transformation of boehmite to α-Al_2O_3 in monolithic samples is inhibited by Cr addition due to stabilization of θ-Al_2O_3 by substitution of Al^{3+} by Cr^{6+} in the tetrahedral sites [45, 46]. However, this effect is not considered to be significant in the present work for three reasons. First, XPS chemical depth profiling [28] has determined that the diffusion distance of Cr into the coating is relatively small (e.g. 400 nm after 16 h heat-treatment time at 800 °C) compared to the thickness of the coatings (3 μm). Second, θ-Al_2O_3 was not observed in any of the thin film XRD patterns. Third, as already discussed, the kinetics and activation energy for the γ-Al_2O_3 to α-Al_2O_3 transformation in the seeded coatings agree well with the published data.

The maximal size of the α-Al_2O_3 grains formed in the coatings was $\sim$ 100 nm at all temperatures (Fig. 8). This suggests that the phase transformation proceeds until all of the parent γ-Al_2O_3 phase has been consumed and the resultant α-Al_2O_3 grains impinge upon each other (Fig. 8(e)). Furthermore, the consistency in maximal grain size between the temperatures suggests that coarsening of the α-Al_2O_3 grains, once the maximal size is attained, does not occur for temperatures up to 950 °C. For a seed concentration of 2.5 wt %, and assuming a uniform seed size of 40 nm, the linear distance between adjacent seed particles is calculated to be 113 nm. Thus, assuming a spherical growth front from each seed particle, the final size of α-Al_2O_3 grains at impingement is 113 nm. This is in good agreement with the size of $\sim$ 100 nm estimated from the TEM micrographs (Fig. 8) and with a size of 90 nm reported for boehmite gels seeded with 5 wt % α-Al_2O_3 particles [47]. This supports the argument that the grain size in the coatings is governed mainly by impingement of the growing grains with little subsequent coarsening at the heat-treatment temperatures used. It is probable that grain coarsening would be significant at higher temperatures [25].

5. Conclusions

Phase evolution in alumina sol gel coatings on biomedical CoCr alloy was studied as a function of heat-treatment temperature and time. The initial deposited phase of boehmite transformed to γ-Al_2O_3 and then to α-Al_2O_3 with increasing temperature. In the case of unseeded coatings, this latter transformation occurred via several alumina transition phases, with α-Al_2O_3 being produced above $\sim$ 1100–1200 °C. The addition of nanometer-sized α-Al_2O_3 particles reduced this temperature to $\sim$ 800 °C and enabled the direct transformation of γ-Al_2O_3 to α-Al_2O_3. It is considered that these particles act as nucleation sites for epitaxial growth of the α-Al_2O_3 phase. The kinetics and activation energy for the phase transformation were similar to those reported for bulk monolithic alumina gels indicating that the same mechanism is operative in both configurations. The Avrami growth parameters indicate that the phase transformation mechanism is diffusion controlled and invariant over the temperature range studied but that growth possibly is constrained by the finite size of the nuclei particles and/or the thickness of the coating. Near complete transformation coincided with physical impingement of the α-Al_2O_3 grains. The grain size at impingement was $\sim$ 100 nm which agreed well with that predicted from the theoretical linear spacing of seed particles in the sol.

Acknowledgments

The authors gratefully acknowledge the financial and technical support of Australian Surgical Design and Manufacture P/L, St Leonards, NSW, Australia.

References

1. N. AL-SAFFAR and P. A. REVELL, *J. Long-Term Effects Med. Implants* **9** (1999) 319.

2. S. CORBETT, M. HUKKANEN, P. HUGHES and J. POLAK, in ''Nitric Oxide in Bone and Joint Disease'', edited by M. Hukkanen, P. Hughes and J. Polak (Cambridge University Press, Cambridge, 1998) p. 178.
3. S. GOODMAN, P. ASPENBERG, Y. SONG, D. REGULA and L. LIDGREN, *Acta Orthop. Scand.* **67** (1996) 599.
4. H. C. AMSTUTZ, P. CAMPBELL, N. KOSSOVSKY and I. C. CLARK, *Clin. Orthop. Rel. Res.* **276** (1992) 7.
5. T. P. SCHMALZRIED, L. M. KWONG, M. JASTY, R. C. SEDLACEK, T. C. HAIRE, D. O. O'CONNOR, C. R. BRASGDON, J. M. KABO, A. J. MALCOLM and W. H. HARRIS, *ibid.* **274** (1992) 60.
6. M. SEMLITSCH and H. G. WILLERT, *J. Eng. Med.* **211** (1997) 73.
7. A. J. ARMINI, S. N. BUNKER and D. M. HUNTINGTON, in ''ASTM STP 1346 Alternative Bearing Surface in Total Joint Replacement'', edited by J. J. Jacobs and T. L. Craig (American Society for Testing and Materials, PA, 1998).
8. H. M. SCHULLER and R. K. MARTI, *Acta Orthop. Scand.* **61** (1990) 240.
9. L. P. ZICHNER and H. G. WILLERT, *Clin. Orthop.* **282** (1992) 86.
10. H. OONISHI, I. C. CLARKE, V. GOOD, H. AMINO, M. UENO, S. MASUDA, K. OOMAMIUDA, H. ISHIMARU, M. YAMAMOTO and E. TSUJI, in ''Bioceramics 15'', edited by B. Ben-Nissan, D. Sher and W. Walsh (Trans Tech Publications, Switzerland, 2003) p. 735.
11. B. J. LIVINGSTON, M. J. CHMELL, D. T. REILLY, M. SPECTOR and R. POSS, in Transactions of the 43rd Orthopaedic Research Society, San Francisco, CA, February 1997, p. 141.
12. Y. S. LI, K. WANG, P. HE, B. X. HUANG and P. KOVACS, *J. Raman Spect.* **30** (1999) 97.
13. R. L. MOORE, G. L. GROBE and J. A. GARDELLA, *J. Vac. Sci. Technol.* **11** (1993) 168.
14. E. N. BUNTING, *Bur. Std. J. Res.* **6** (1931) 947.
15. D. M. ROY and R. E. BARKS, *Nature (London) Phys. Sci.* **235** (1972) 118.
16. S. S. KIM and T. H. SANDERS, *J. Am. Ceram. Soc.* **84** (2001) 1881.
17. I. LEVIN and D. BRANDON, *ibid.* **81** (1998) 1995.
18. L. PACH, R. ROY and S. KOMARNENI, *J. Mat. Res.* **5** (1990) 278.
19. S. J. WILSON, *J. Solid State Chem.* **30** (1979) 247.
20. B. E. YOLDAS, *J. Am. Ceram. Soc.* **65** (1982) 387.
21. M. KUMAGAI and G. L. MESSING, *ibid.* **68** (1985) 500.
22. J. L. McARDLE and G. L. MESSING, *ibid.* **69** (1986) C98.
23. C. S. OH, G. TOMANDL, M. H. LEE and S. C. CHOI, *J. Mat. Sci.* **31** (1996) 5321.
24. W. A. YARBROUGH and R. ROY, *J. Mat. Res.* **2** (1987) 494.
25. J. M. MCARDLE and G. L. MESSING, *J. Am. Ceram. Soc.* **76** (1993) 214.
26. H. C. KAO and W. C. WEI, *ibid.* **83** (2000) 362.
27. A. M. BELTRAN, in ''Superalloys II'', edited by C. T. Sims, N. S. Stoloff and W. C. Hagel (Wiley and Sons, NY, 1987) p. 135.
28. I. J. BAE and O. C. STANDARD, University of New South Wales, Sydney, Australia (2003) (unpublished work).
29. ASTM F75-92, ''Cast Co–Cr–Mo Alloy for Surgical Implant Applications'' (American Society for Testing and Materials, West Conshohocken, PA, 1996).
30. B. E. YOLDAS, *J. Appl. Chem. Biotech.* **23** (1973) 803.
31. J. W. CHRISTIAN, ''Transformations in Metals and Alloys, 2nd edn. Part I Equilibrium and General Kinetic Theory'' (Pergamon, Oxford, 1975).
32. Card No. 21-1307, Powder Diffraction File 2 (International Centre for Powder Diffraction, Newtown Square, PA, USA, 2003).
33. Card No. 10-0425, Powder Diffraction File 2 (International Centre for Powder Diffraction, Newtown Square, PA, USA, 2003).
34. Card No. 16-0394, Powder Diffraction File 2 (International Centre for Powder Diffraction, Newtown Square, PA, USA, 2003).
35. Card No. 23-1009, Powder Diffraction File 2 (International Centre for Powder Diffraction, Newtown Square, PA, USA, 2003).
36. Card No. 42-1468, Powder Diffraction File 2 (International Centre for Powder Diffraction, Newtown Square, PA, USA, 2003).
37. C. S. OH, G. TOMANDL, M. H. LEE and S. C. CHOI, *J. Mater. Sci.* **31** (1996) 5321.
38. P. A. BADKAR and J. E. BAILEY, *ibid.* **11** (1976) 1794.
39. S. J. WILSON and J. D. C. MCCONNELL, *J. Solid State Chem.* **34** (1980) 315.
40. T. W. SIMPSON, Q. WEN, N. YU and D. R. CLARKE, *J. Am. Ceram. Soc.* **81** (1998) 61.
41. J. M. MCARDLE and G. L. MESSING, *ibid.* **72** (1989) 864.
42. R. A. SHELLEMAN, G. L. MESSING and M. KUMAGAI, *J. Non-Cryst. Solids* **82** (1986) 277.
43. M. E. BROWN, D. DOLLIMORE and A. K. GALWEY, in ''Reactions in the Solid State, Comprehensive Chemical Kinetics'', Vol. 22, edited by C. H. Bamford and C. F. H. Tipper (Elsevier, Amsterdam, 1980).
44. F. S. HAM, *J. Phys. Chem. Solids* **6** (1958) 335.
45. T. TSUCHIDA, R. FURUICHI, T. ISHII and K. ITOH, *Thermochem. Acta* **64** (1983) 337.
46. G. C. BYE and G. T. SIMPKIN, *J. Am. Ceram. Soc.* **57** (1974) 367.
47. S. RAJENDRAN, *J. Mater. Sci.* **29** (1994) 5664.

Received 14 January
and accepted 29 March 2004